Gold Bull (2014) 47:141–151
DOI 10.1007/s13404-014-0135-z

ORIGINAL PAPER

Evolution and investigation of copper and gold ball bonds in extended reliability stressing

C. L. Gan · F. C. Classe · B. L. Chan · U. Hashim

Published online: 29 March 2014

Abstract This paper discusses the microstructure evolution of copper (Cu) and gold (Au) ball bonds after various extended reliability stresses such as biased highly accelerated temperature and humidity test (HAST), unbiased highly accelerated temperature and humidity test (UHAST), temperature cycling (TC), and high temperature storage life (HTSL) in BGA package. Objective of this study is to study the microstructure evolution and changes after long hours and long cycles of component reliability stressing and its predicted failure mechanisms and to determine the long-term reliability comparison with combination of bonding wires in HAST, UHAST, and TC. Secondary electron microscopy (SEM) and energy dispersive X-ray (EDX) have been carried out to understand the respective microstructure of failed samples in HAST, UHAST, TC, and HTSL long-term reliability failures. Respective failure mechanisms of copper and gold ball bonds carrion under HAST and UHAST, ball bond lifting in TC and HTSL have been analyzed and proposed. The evolution of surface morphology, including copper and gold ball bond micro cracking, gold ball bond Kirkendall microvoiding and intermetallic compound (IMC) formation, was studied in FBGA package with copper and gold ball bonds during various reliability stresses. Biased HAST, UHAST, TC, and HTSL mechanisms were proposed to explain the observed morphological changes and the resulting ball bond wear out modes after extended reliability stresses. Weibull reliability analyses have been established to compare the performance of copper and gold ball bonds under humid and dry environmental tests.

Keywords Microstructure evolution · Copper and gold ball bonds · Failure mechanisms · SEM · EDX analysis · Extended reliability · Weibull plot

C. L. Gan (✉) · F. C. Classe · B. L. Chan
Spansion (Penang) Sdn Bhd, Phase II Free Industrial Zone,
Penang 11900 Bayan Lepas, Malaysia
e-mail: chong-leong.gan@spansion.com

C. L. Gan · U. Hashim
Institute of Nanoelectronic Engineering (INEE), Universiti Malaysia
Perlis, Perlis 01000, Kangar, Malaysia

Introduction

Gold and copper wire bondings are two most common bonding techniques used in microelectronic packaging in semiconductor industry. Recently, copper wire bonding appears to be the alternate materials and various engineering studies on copper wire development have been reported [1]. Technical barriers and reliability challenges of Cu wire bonding in microelectronics packaging are well identified [2–11]. Au-Al microstructure evolution and intermetallic compound (IMC) formation is widely studied by Karpel et al. [12]. Two types of failures occurred during annealing: crack formation at the bond periphery due to an increase in volume during intermetallic growth and the formation of stresses; and oxidation of the $AlAu_4$ phase adjacent to the Au ball, which resulted in the formation of continuous cracks between the Au ball and the intermetallic region [10]. Drozdov et al. [13, 14] evaluated CuAl IMC formation on as-bonded stage and post annealing to study the interface composition and morphology of copper wire bonds heat-treated at 175 °C for 2, 24, 96, and 200 h in argon. The main intermetallic phase was Al_2Cu, which was found to grow via solid state diffusion. In specimens heat-treated for 96 and 200 h, the Al_4Cu_9 phase was also detected. Void formation at the Al–Cu bonds heat-treated up to 200 h was not found to be a source of bond failure. Xu C et al. [15] studied oxidation behavior of two types of bulk gold aluminides, $AuAl_2$, and Au_4Al, using thermogravimetry. Xu H et al. [16, 17] characterized behavior of aluminum oxide, intermetallics, and voids in

Cu–Al wire bonds. Zeng Y et al. [18] plotted Pourbaix (Eh–pH) diagrams of Al–Cu alloys (instead of pure metals) are generated on the basis of critical assessment of thermodynamic data. The Eh–pH diagram is used to conduct comprehensive studies on the thermodynamic equilibrium of Cu–Al bonding at humid environment with chlorine.

Cu ball bond is more susceptible to moisture corrosion compared to gold ball bonds and undergo different corrosion mechanisms in microelectronic packaging [19–21]. There are different ball bonds corrosion mechanisms of Au and Cu ball bond under humid reliability test. Uno T [21] reported CuAl IMC interfacial corrosion under HAST environmental test. Yamaji Y et al. [22] and Su P et al. [23] reported similar CuAl IMC interfacial corrosion post HAST and UHAST tests and effects of pH of molding compounds on HAST failure rates. Lu YH et al. [24] observed the growth rates of IMCs in Pd-coated Cu wire bonds are very sensitive to temperature, but the sequence of IMC formation remains the same for temperature below 350 °C. Pd atoms in the Pd-coated Cu wire do not participate in the interfacial reaction, and have no marked effect on the growth rate of IMCs. Gan et al. conducted studies on effects of bonding wires on UHAST and TC reliability and found Au with better UHAST reliability compare to Cu wire [25–31]. Au ball bond is well known with its Au atomic diffusion into Al metallization and caused resistive ball bonds with non-optimized bonding parameter [1, 25]. The interdiffusion between Au and Al across a thermally exposed Au-Al ball bond causes the movement of the void line towards the Au bump and shows that Au interdiffuses faster than Al. Although the movement of the void line appears to be associated with movement of the Au_4Al or Au_8Al_3 interface, it is actually analogous to the Kirkendall microvoiding. Yu CH et al. [32] studied HTSL failure mechanism of Cu ball bond after aging at 205 °C in air from 0 h to 2,000 h. The cracks grew towards the ball bond center with an increase in the aging time, and the Cl ions diffused through the crack into the ball center. This diffusion caused a corrosion reaction between the Cl ions and the Cu–Al intermetallic phases, which in turn caused copper wire bonding damage [32].

Experimental procedures

Specimen preparation

Copper wires were bonded on top of silicon wafers coated with thermally grown SiO_2 and covered by uniform aluminum (Al) metallization. The Al metallization consisted of 0.5 wt% Cu and 1 wt% Si. Materials used include 0.8 mil Pd-coated Cu wire (Cu) and 4 N (99.99 % purity) gold (Au) wire, 90 nm and 110 nm flash devices packaged into fortified fine-pitch BGA packages, with green (<20 ppm chloride in content) molding compound and substrate. Thermosonic ball bonding of each Si die was performed at 175 °C for an approximate time of 18 s per device with a pre-heat and post-heat of 18 s at 150 °C. The bonding parameters were optimized to ensure zero pad peals, which is an essential condition for successful copper wire bonding. In order to ensure uniform and symmetric bonds, free air balls at the Cu wire tip were formed by melting the tips of the Cu wires in a reducing atmosphere (95 % N_2, 5 % H_2) prior to the bonding stage.

The corresponding stress tests and its conditions are tabulated in Table 1. Extended reliability stresses include biased HAST (130 °C, 85 %RH, 3.60 V biasing voltage), unbiased HAST (130 °C, 85 %RH), temperature cycling (−40 °C to 150 °C), and HTSL (150 °C and 200 °C). All direct material used in this evaluation study for the 90 nm and 110 nm, flash device (with top Al metallization bondpad) for packaging purpose. Forty-five units of Au and Pd-coated Cu wire bonded on fine-pitch 64-ball BGA packages are subjected for 150 °C aging temperature. Electrical testing was conducted after each hours and cycles of stress to check Au and Cu ball bond integrity in terms of its high temperature ball bonds reliability with various aging conditions. The package construction of test vehicle, FBGA 64 as depicted in Fig. 1, is assembled with gold or copper wires.

Prior to biased HAST, UHAST and TC stresses, the electronic packages were subjected to preconditioning (30 °C, 60 %RH) for 192 h in a temperature and humidity chamber, followed by three cycles of reflow at 260 °C by using reflow chamber as per JEDEC IPC-STD 020 [35]. After preconditioning and electrical test, samples were loaded in respective HAST, UHAST, and TC chambers according to the stress conditions as tabulated in Table 1. After each read point, electrical opens, shorts, and device datasheet functionality was verified by using a commercial electrical tester. Cu and Au ball bonds microstructure analysis were measured by using secondary electron microscopy (SEM) to understand the morphology and microstructure evolution. Composition analysis on failed samples were determined by using energy dispersive X-ray (EDX) on FBGA 64 package with different sets of extended reliability stresses. Wear out reliability tests were conducted on HAST, UHAST, and TC package reliability stresses to predict its reliability margins of Au and Cu wires used in FBGA package. The time and cycles-to-failures reliability modeling can be predicted based on the stress-to-failures in respective reliability stresses [33].

Table 1 Summary of extended reliability matrix (for Au and Cu wires)

Extended reliability stresses	Test conditions	Sample size
Biased HAST	85 %RH, 110 °C, 3.6 V	80
Unbiased HAST	85 %RH, 130 °C	80
TC	−40 °C to 150 °C	80
HTSL	150 °C, 200 °C	45

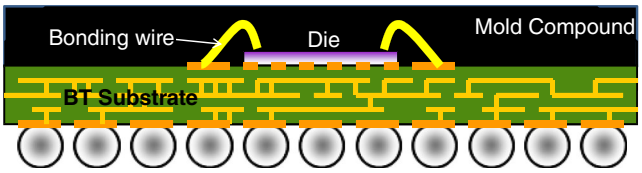

Fig. 1 FBGA 64 package constructions with Cu and Au wires used in reliability sample preparation

Result and discussion

Ball bond corrosion under highly humidity and temperature test

Biased HAST test

In order to obtain information regarding the Al–Cu interface composition after HAST or UHAST tests, CuAl and AuAl samples were studied using EDX. EDX analysis was conducted using FEI Tecnai microscopes, following the standard procedure. In order to ensure acquisition of the signal from a selected region, the specimen was tilted 15° towards the EDX detector. Typical CuAl IMC microcracking is found for the HAST 2,000 h electrical open failure (see Fig. 2).

Figure 3 shows representative SEM cross section and EDX analysis of failed Cu ball bond. EDX analysis on the micro crack at the edge of Cu ball bond indicates presence of O and Cl peaks. This proves the hydrolysis of CuAl IMC under UHAST moist conditions and Cl peak is originated from $AlCl_3$. The trace Cl^- is usually found in epoxy mold compound. Tables 2 and 3 tabulates the summary of EDX analysis of Au and Cu ball bonds.

Figure 4 reveals SEM micrograph of HAST 2,000 h open found on Au ball bond and presents SEM micrographs taken the periphery of a bond subjected for HAST 2,000 h. The intermetallic coverage of the Au–Cu interface is not complete. Regions at the interface with no intermetallics can still be found. The intermetallics found at the bond periphery are less uniform than those found along the whole gold ball bonds. The intermetallics found at the left side of gold ball bond are more continuous. Voiding between the gold ball and the intermetallics located at the bond periphery can be detected. EDX analysis (in Table 2) confirmed presence of O peak and this might be induced by hydrolysis of Au_4Al into Al_2O_3 (see Eq. 3).

Unbiased HAST test

UHAST test is pretty similar to biased HAST test except is without biasing condition (85 %RH, 130 °C). Corrosion is typically found after long hours of UHAST test. Figure 5 presents SEM micrograph of failed Cu ball bond (electrical open) after 3,000 h of UHAST stress. EDX analysis on failing Cu ball bond shows higher percentage of O and Cl peaks compared to good ball bond (see Table 2). The source of Cl^- could be originating from the non-green molding compound used in assembly of FBGA 64 and corroded the Cu ball bond under highly temperature and humidity stresses such as UHAST or HAST.

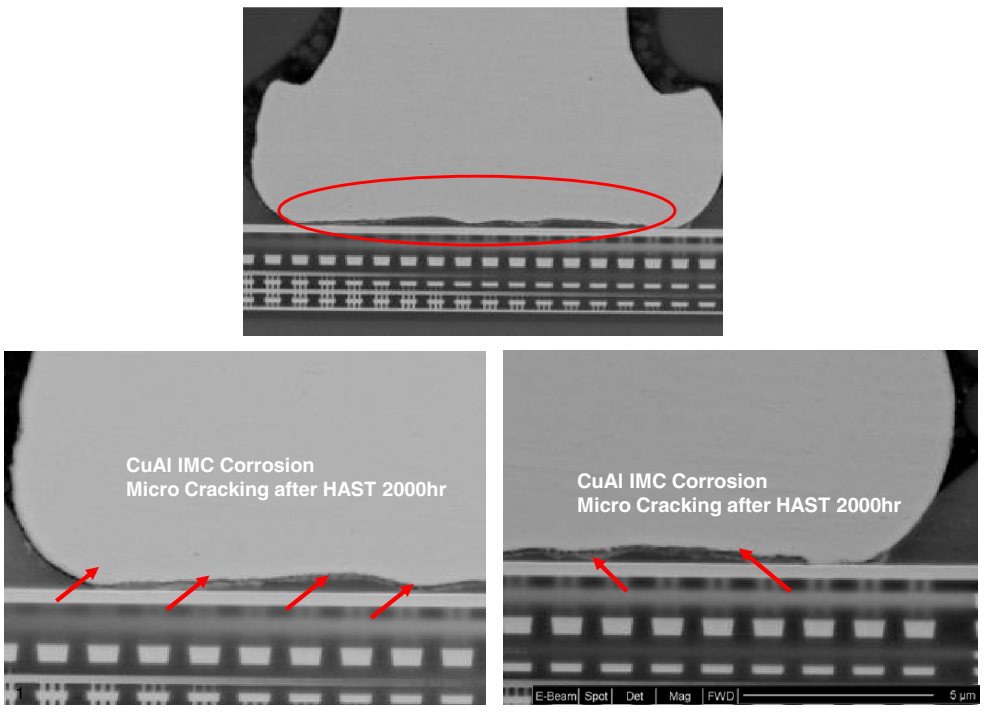

Fig. 2 Cu ball bond corrosion found after biased HAST 2,000 h. CuAl IMC interface microcracking found beneath Cu ball bond in extended hours of HAST failure

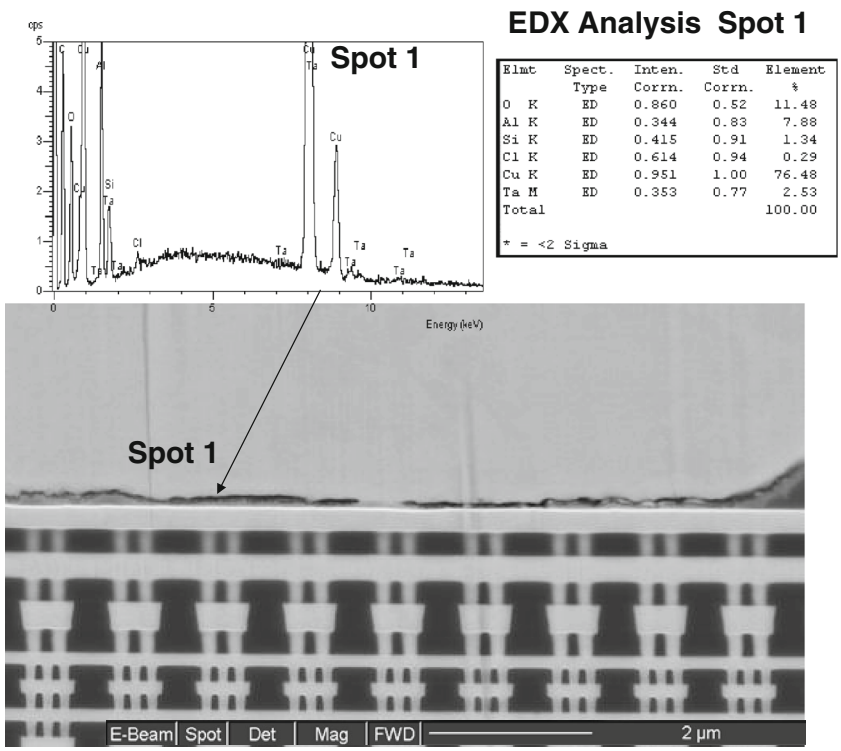

Elmt	Spect. Type	Inten. Corrn.	Std Corrn.	Element %
O K	ED	0.860	0.52	11.48
Al K	ED	0.344	0.83	7.88
Si K	ED	0.415	0.91	1.34
Cl K	ED	0.614	0.94	0.29
Cu K	ED	0.951	1.00	76.48
Ta M	ED	0.353	0.77	2.53
Total				100.00

* = <2 Sigma

Fig. 3 EDX analysis shows presence of Cl^- content at the CuAl IMC interfacial microcracking region. Cu ball bond corrosion found after biased HAST 2,000 h

Ball bond microcracking under dry environmental stress

Temperature cycling test

Figure 6a presents SEM micrograph of CuAl IMC microcracking after undergoing extended temperature cycling (TC) stress of 9,500 cycles of −40 °C to 150 °C. Obvious molding compound to die passivation delamination is observed across the row of failing Cu ball bonds. This indicates the mismatches of coefficient of thermal expansion (CTE) between molding compound and silicon die which induced the CuAl IMC microcracking after extended cycles of TC. Figure 6b shows closed up failed Cu ball bond after TC 9,500 cycles and full separation of CuAl IMC beneath Cu ball bond. EDX analysis on site 1 and site 2 near the CuAl IMC interfacial microcracking shows presence of C, Cu, O, Si, and Al elements without Cl^- element (see Fig. 6b). Table 4 tabulates the EDX analysis comparing failing Au and Cu ball bond after TC 9,500 cycles.

High temperature storage life test

Specimens heat-treated in nitrogen for more than 3,000 h at 150 °C Figure 7a, b presents SEM micrographs of failed Cu ball bonds after aged for 3,500 h at 150 °C. We found CuAl IMC full separation and microcracking along beneath Cu ball bonds at the edge and also center regions of CuAl IMC. EDX area scan reveals presence of O, Al, Si, and Cu elements at the edge of failed Cu ball bond. No signature of halide element such as Cl (see Fig. 7c) since HTSL is conducted in a dry environmental chamber with nitrogen purging gas.

Figure 8 indicates the uneven AuAl IMC layer formation after aging for 3,500 h at 150 °C. The SEM micrographs show the Au HTSL 3,500 h opens. Variation of thicknesses of AuAl IMCs is noted due to the faster Au atom diffusion into Al metallization on Al bondpad. Hence, thicker AuAl IMC will be found in HTSL stress, and Kirkendall microvoiding is observed after long aging time in Au ball bonds (see Fig. 8).

Representative EDX analysis of failed Cu and Au ball bonds after 3,500 h of HTSL at 150°C is shown in Table 5

Table 2 EDX analysis of failed Cu and Au ball bonds after HAST 2,000 h open failures

Sample	Element (atomic %)						
	Au	Cu	O	Al	Si	Ta	Cl
Au ball	32.15	–	24.76	43.15	–	–	–
Cu ball	–	76.48	11.48	7.88	1.34	2.53	0.29

Table 3 EDX analysis of failed Cu and good Cu ball bonds after UHAST 3,000 h

Sample	Element (atomic %)						
	Au	Cu	O	Al	Si	Ta	Cl
Good Cu ball	–	83.14	1.48	11.02	0.98	3.38	–
Failed Cu ball	–	78.28	8.64	8.17	1.89	2.40	0.68

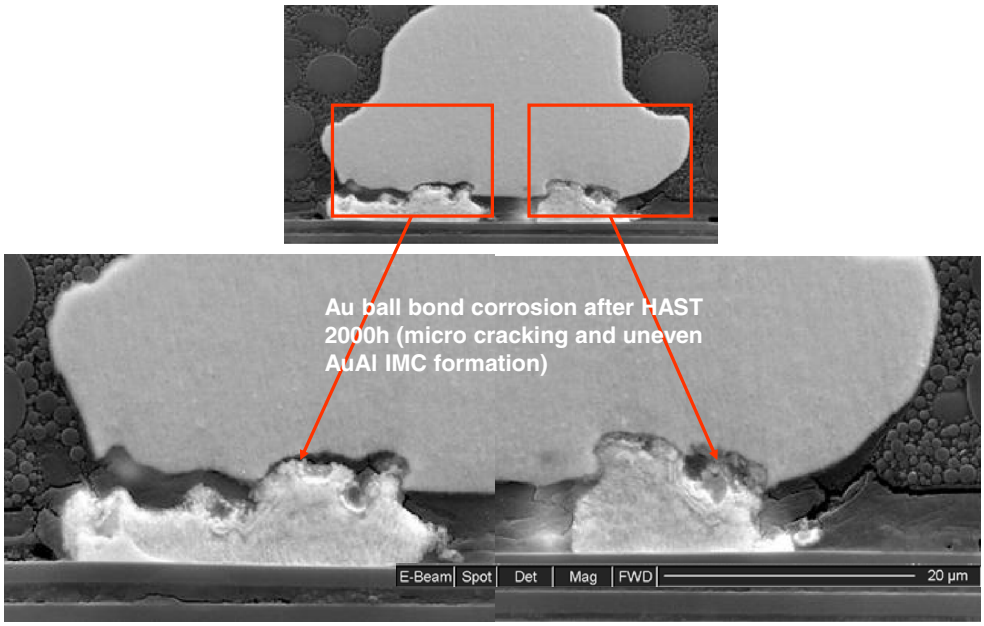

Fig. 4 Au ball bond corrosion found after biased HAST 2,000 h. Thicker AuAl IMC is formed unevenly beneath Au ball bond. Microcracking is observed between Au ball bond and AuAl IMC. EDX analysis reveals presence of Au, O, and Al elements

whereby no presence of Cl^- ion in both failing Au and Cu ball bonds. This is noted as HTSL test is conducted in a dry environment condition at 150°C. As noted in our previous report [34, 35], discontinuous intermetallics were found in aged HTSL specimens on Au and Cu ball bonds. The predicted HTSL wear out mechanisms are illustrated in Fig. 11.

Cu and Au ball bond corrosion (biased HAST and unbiased HAST)

CuAl IMC growth mechanism is slightly different from AuAl IMC in microelectronic packages. The IMC between Cu wire and Al pad can be distinguished into five types, as in the case of Au wire. However, only two IMC, Cu_9Al_4 and $CuAl_2$, can be typically observed because the CuAl IMC forms very slowly and it is very thin in Cu ball bond IMC growth. CuAl IMC will be formed thicker at the edge of Cu ball bond compared to the center of Cu ball bond. This is mainly due to the thermo-compression effect during capillary compression onto Al bondpad during wire bonding induced by capillary compression.

Moisture in HAST or UHAST chamber will attack Cu ball bond at both edges of Cu ball bonds. Trace Cl^- ion from molding compound will corrode the thin CuAl IMC layer beneath Cu ball bond and hydrolysis of CuAl IMC will occur (see Eq. 1). CuAl IMC microcracking will occur as a result of hydrogen outgassing or embrittlement (as in Eq. 2). Hydrolysis of CuAl IMC will form a brittle IMC, still conductive in Cu ball bond but resistive and will reach wear out opens (lifted ball bond after corrosion) after extended reliability stressing under HAST or UHAST (see Fig. 9).

$$Cu_9Al_4 + 6H_2O \rightarrow 2(Al_2O_3) + 6H_2 + 9Cu(\text{out gassing}) \quad (1)$$

$$CuAl_2 + 3H_2O \rightarrow Al_2O_3 + Cu + 3H_2(\text{out gassing which might cause IMC cracks}) \quad (2)$$

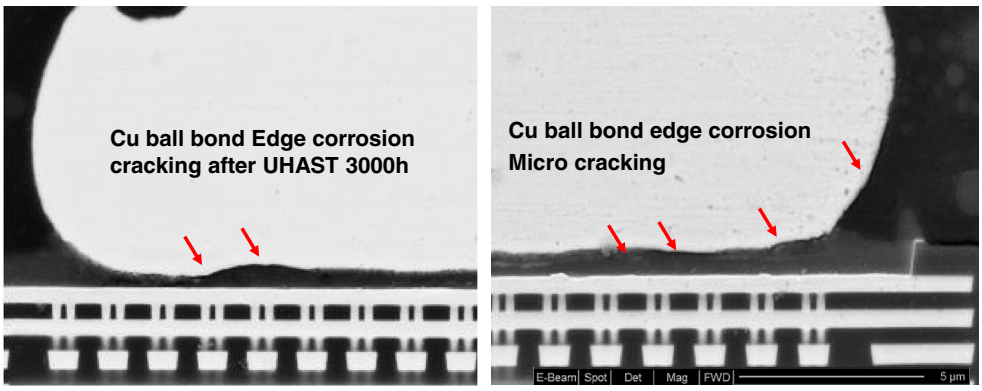

Fig. 5 Cu ball bond corrosion found after unbiased HAST 3,000 h. Microcracking is observed at the edge of Cu ball bond region. EDX analysis reveals presence of Cu, O, Cl, and Al elements

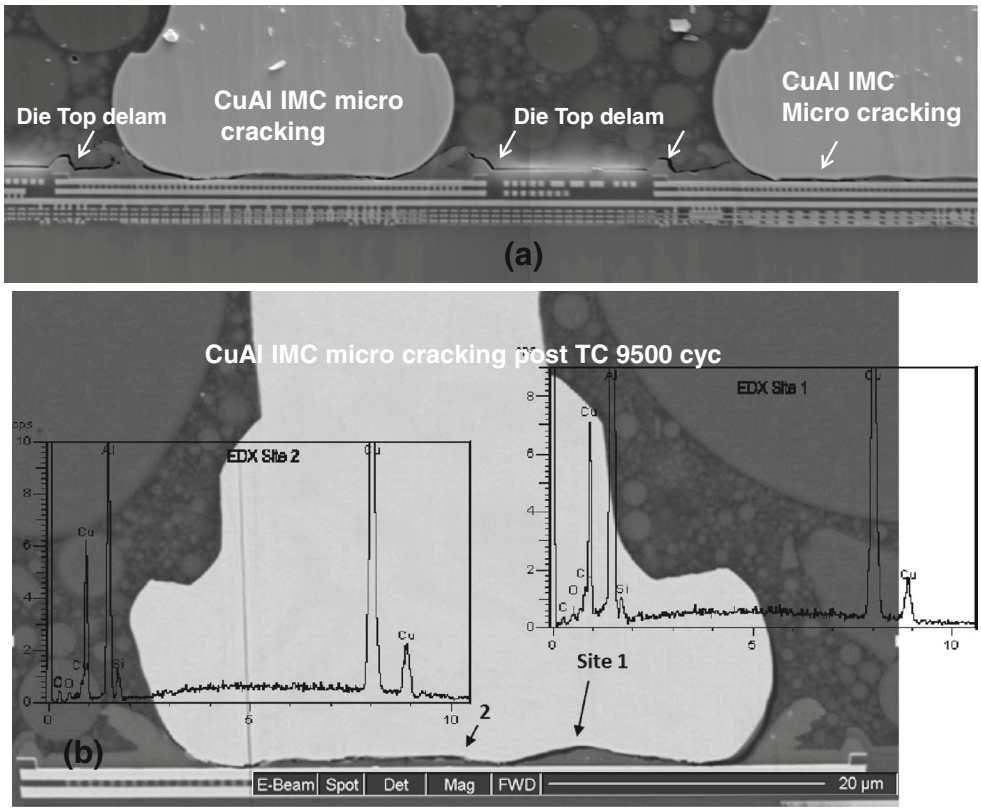

Fig. 6 Cu ball bond microcracking is observed after TC 9,500 cycles (**a**). Mold compound to die interfacial delamination is found and might be the factor induced CuAl IMC microcracking. EDX analyses reveal presence of C, Cu, O, Si, and Al elements without Cl^- element (**b**)

Au ball bond undergoes a slightly different corrosion mechanism in HAST or UHAST reliability stressing. Moisture in HAST or UHAST chamber will penetrate from the edge of Au ball bond after long hours of HAST and UHAST stressing. AuAl IMC will react with moisture and form Al_2O_3 and hydrogen outgassing (as shown in Eq. 3). Hydrogen gas evolution due to moisture in contact with intermetallics has been extensively documented and is one of the known causes of embrittlement [10]. Stress-induced microcracking will cause AuAl microcracking together with the formation of Kirkendall microvoiding which results in uneven AuAl IMC formation (refer Fig. 4). Lifted Au ball bond will occur after long hours of HAST or UHAST stress and this is typical wear out failure (as shown in Fig. 10).

$$2Au_4Al + 3H_2O \rightarrow Al_2O_3 + 8Au + 6H \quad (3)$$

Table 4 EDX analysis of failed Cu and Au ball bonds after TC 9,500 cycles

Location	Element (atomic %)						
	Au	Cu	O	Al	Si	C	Cl
Au ball	38.25	–	1.76	59.99	–	–	–
Cu ball	–	77.58	2.11	13.74	3.74	2.83	

Au and Cu ball bond microcracking in HTSL

Au ball bond is found with higher IMC growth rate at least 5× compared to Cu ball bond in HTSL aging test [1, 25]. Hence, there is slightly different HTSL failure mechanism after long duration of aging stress in Au and Cu ball bonds. Both CuAl and AuAl IMCs are formed in long hours of HTSL test except more uniform AuAl IMC formation compared to CuAl. Thicker CuAl IMC is formed at the edge of Cu ball bond (see Figs. 2 and 7c). AuAl IMC is observed with more uniform and thicker (as indicated in Fig. 8) but Kirkendall microvoiding will occur which might induce AuAl IMC microcracking (Fig. 11b). HTSL wear out opens occur as lifted ball bonds for both Au and Cu balls except with Kirkendall microvoiding in Au ball bonds (Fig. 11a, b, respectively).

Au and Cu ball bond microcracking in TC

Table 6 tabulates coefficient of thermal expansion (CTE) for materials used in package bills of materials in FBGA 64. The mismatch in CTE between Cu (17.8 ppm/°C) and Au ball bond (14.2 ppm/°C) to the silicon die (3.0 ppm/°C) induced different thermal expansions and contraction rates in the temperature cycling test. The CTE mismatch between Au and Cu ball

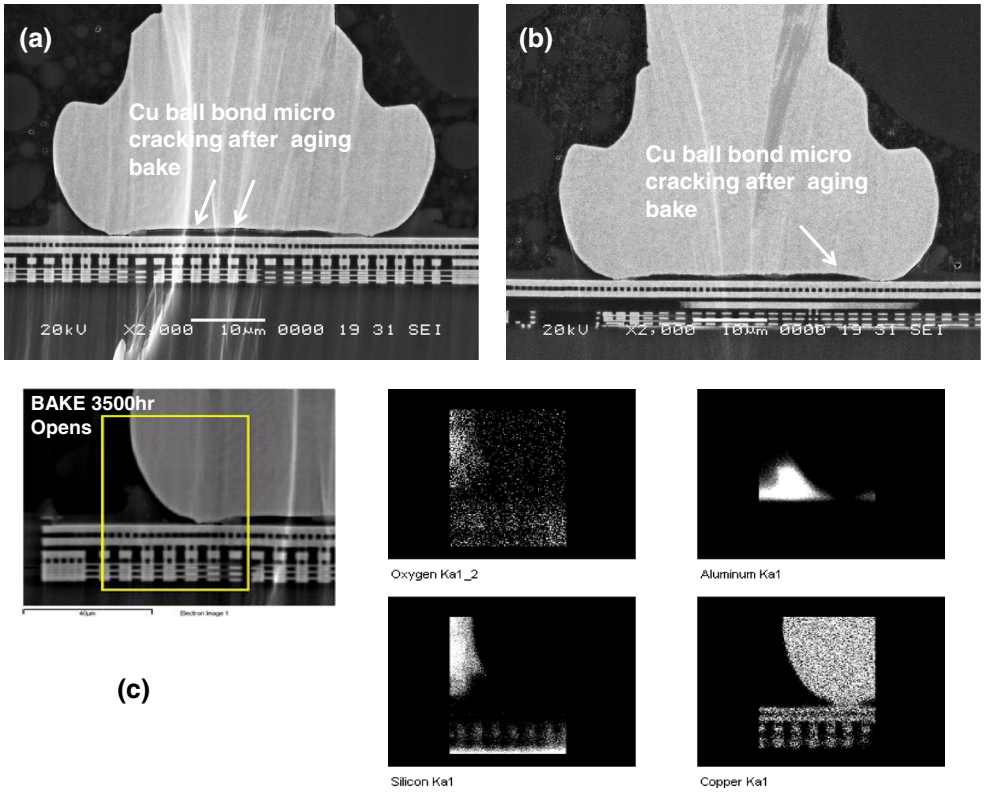

Fig. 7 Cu ball bond IMC microcracking is found after HTSL 3,500 h of stressing (**a**, **b**). EDX area scan reveals presence of O, Al, Si, and Cu elements at the edge of failed Cu ball bond. No signature of halide element such as Cl (**c**)

bonds with Al bondpad of silicon die will impose different thermal expansion rates during hot cycles (150 °C) and contraction rates during cold cycles (−40 °C). IMC formation initiated at the edge of the ball bond (due to the ball bond pressing force by bonding capillary) and microcracking will be induced after long cycles of thermal cycling effects. The microcracking occurs in between ball bond IMC (as shown in Fig. 12). This predicted TC mechanism also correlated to SEM images as indicated in Fig. 12.

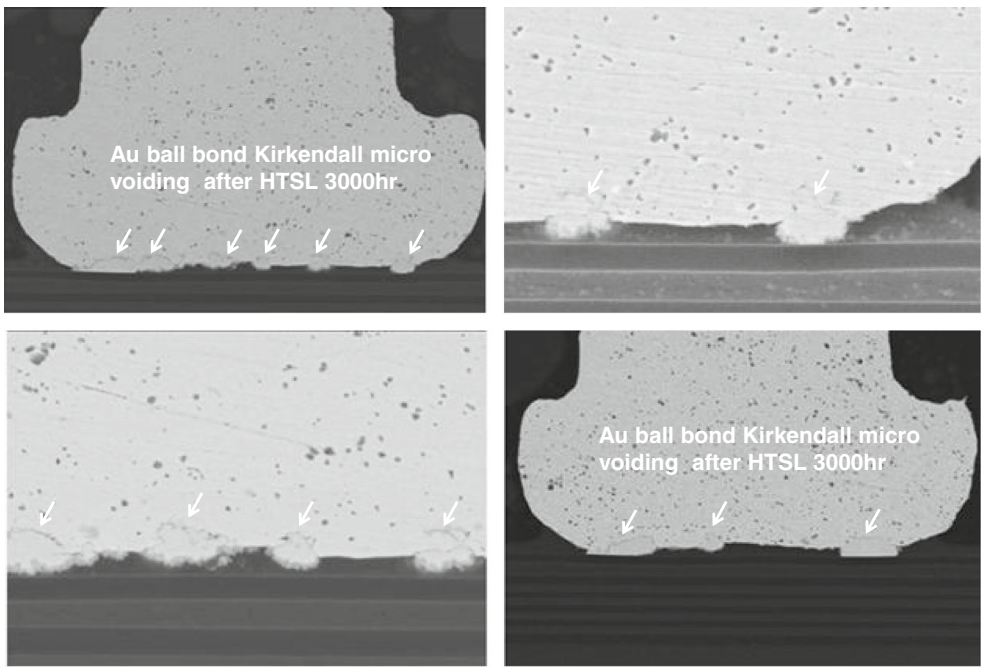

Fig. 8 Au ball bond with uneven AuAl IMC formation and Kirkendall microvoiding are found along the Au ball bond after HTSL 3,000 h at 150 °C aging condition. Hairline cracking is observed along the Kirkendall microvoiding region

Table 5 EDX analysis of failed Cu and Au ball bonds after HTSL 3,500 h

Location	Element (atomic %)					
	Au	Cu	O	Al	Si	Cl
Au ball	48.65	–	0.97	50.38	–	–
Cu ball	–	77.58	2.11	13.74	3.74	–

Extended reliability analysis of Au and Cu ball bonds

Humidity reliability analysis (UHAST)

All package reliability plots belong to wear out reliability mode in bathtub curve since its shape parameter (ß) is more than 1.0. Au ball bonds show better UHAST package reliability performance with higher mean-time-to failure hours (t_{50}) and characteristics life ($t_{63.2}$, η) in UHAST reliability plot (fitted to Weibull distribution) compared to Cu ball bonds. Figure 13 illustrates a Cu ball bond with lower package reliability margin and usually more susceptible to Cu moisture corrosion test under UHAST condition. This has been reported in our previous literature works [8, 25–27, 31]. Cu ball bond has a layer of Pd coated on low-corrosive resistance Cu wire which inhibits moisture ball bond corrosion in UHAST conditions (130 °C, 85 %RH). However, Au wire is well known with corrosion resistant material and shows higher hours-to-failure in UHAST wear out reliability plot (Fig. 13).

Dry environmental reliability analysis (TC)

Cu ball bonds is found with higher mean-time-to failure hours (t_{50}) and characteristics life ($t_{63.2}$) in TC reliability plot (fitted to Weibull distribution), as indicated in Fig. 14. Apparently, Cu performs well under dry conditions in the TC cycling test (−40 °C to 150 °C). In this case, we observe Cu ball bonds withstand higher cycle-to-failure compared to Au ball bonds in TC stress test conditions.

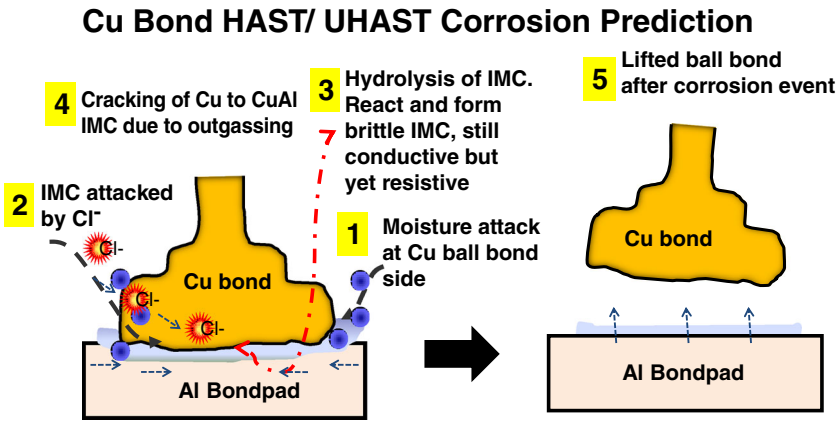

Fig. 9 Proposed CuAl IMC corrosion mechanism on 110 nm device FBGA 64 package after extended hours of biased HAST or unbiased HAST stressing [31]

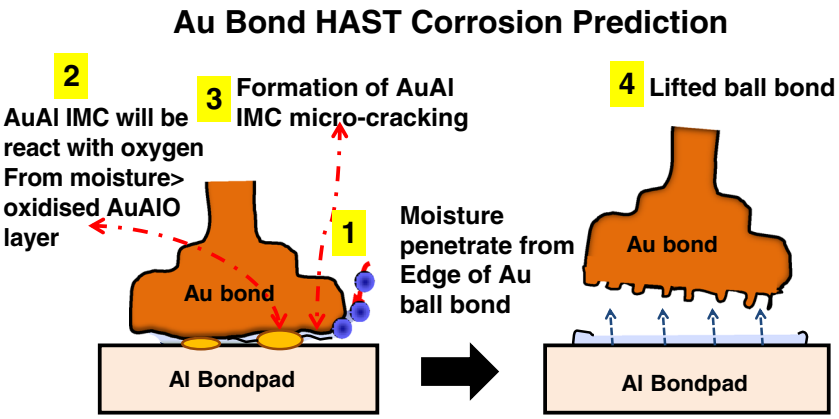

Fig. 10 Proposed AuAl IMC Kirkendall microvoiding mechanism and induced opens after long aging hours on 110 nm device FBGA 64 package [31]

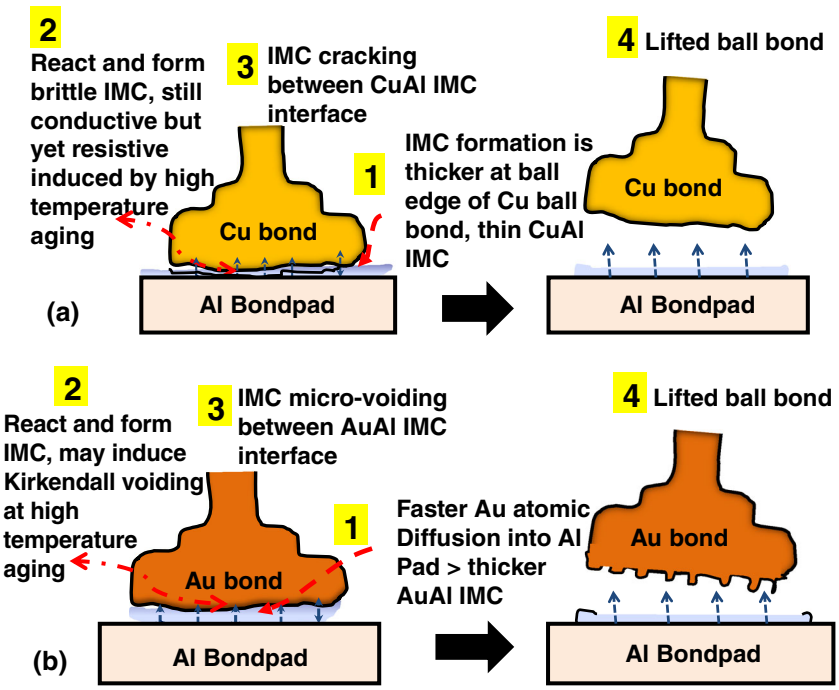

Fig. 11 Schematic representation of Cu ball bond microcracking after long hours of HTSL stressing (**a**) and Kirkendall microvoiding as a function of aging hours in Au ball bond (**b**)

Table 6 Key material characteristics of epoxy mold compound (EMC) A and B

Material	Units	CTE (coefficient of thermal expansion)
Au	ppm/°C	14.2
Cu	ppm/°C	17.8
Silicon	ppm/°C	3.0
Al	ppm/°C	22.2

Summary and conclusions

The purpose of this research is to investigate and understand the microstructural evolution of Au and Cu ball bonds in extended reliability stressing such as HAST, UHAST, TC, and HTSL. To achieve this goal, both AuAl and CuAl intermetallic growth was studied at elevated temperatures in HTSL. In our study, respective failure mechanisms of copper and gold ball bonds carrion under HAST and UHAST, ball bond lifting in TC and HTSL have been analyzed and proposed. The evolution of surface morphology, including copper and gold ball bond microcracking, gold ball bond Kirkendall

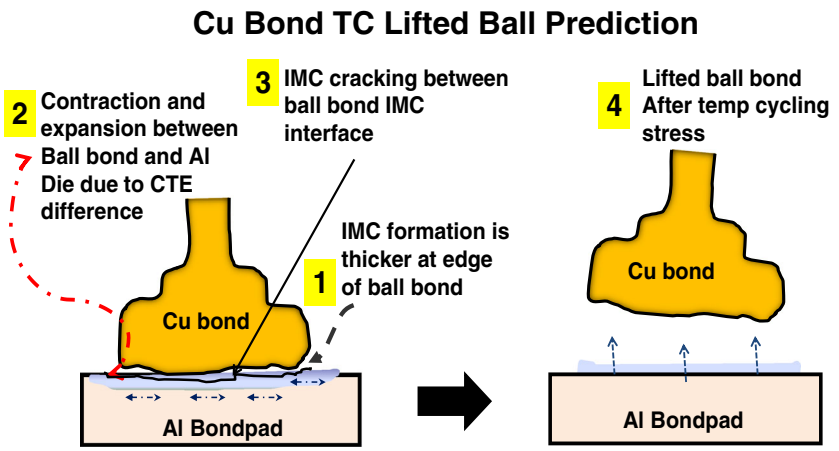

Fig. 12 Proposed Cu ball bond microcracking induced by different rate of contraction and expansion between Cu bond and silicon die after extended temperature cycling

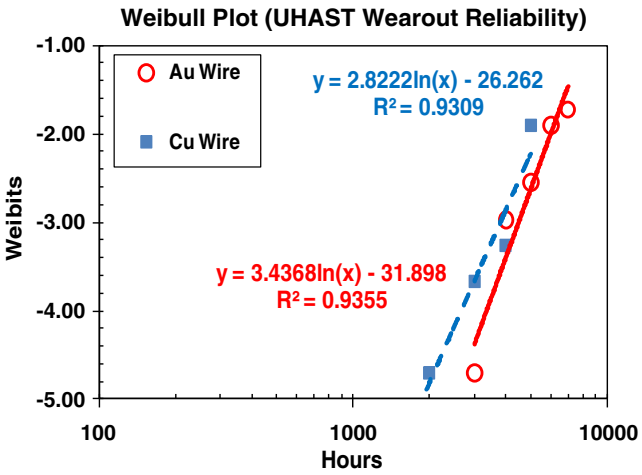

Fig. 13 Obtained Weibull plotting of Au and Cu ball bonds in unbiased HAST reliability stress with different epoxy mold compounds (EMC) [26, 31]

microvoiding and IMC formation, was studied in FBGA package with copper and gold ball bonds during various reliability stresses. Au ball bonds show superior extended UHAST reliability than Cu ball bonds for both mold compounds A and B (see Fig. 13). This could be due to Au is more stable and higher corrosion resistance under moisture UHAST conditions compared to Cu ball bonds. We observed Cu ball bonds with higher TC extended reliability performance (higher t_{first}, t_{50}, and $t_{63.2}$) compared to Au ball bonds in FBGA 64 package of both mold compounds A and B (Fig. 14). The effect of wire type is not the key factor affecting the TC reliability performance but we observed higher extended reliability performance in Cu ball bonds compared to Au ball bonds.

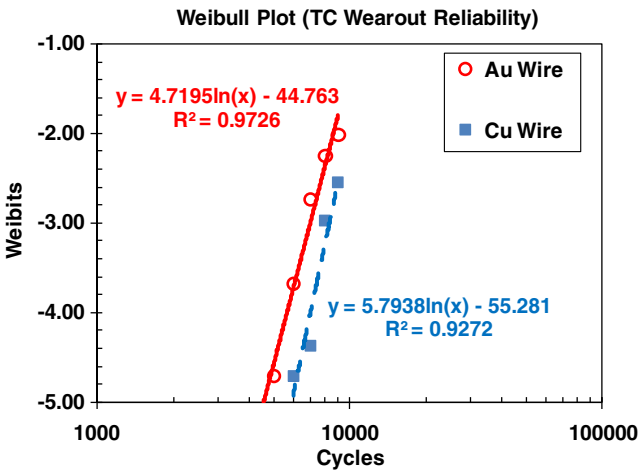

Fig. 14 Obtained Weibull plotting of Au and Cu ball bonds in extended TC reliability stress with different epoxy mold compounds (EMC) [26, 31]

Acknowledgement The authors would like to take this opportunity to thank Spansion management for their management support for the paper publication.

References

1. Harman GG (1999) Wirebonding in microelectronic: materials, processes, reliability and yield, 2nd edn. McGraw Hill, New York
2. Chauhan P, Zhong ZW, Pecht M (2014) Copper wire bonding, 1st edn. Springer, New York
3. Chauhan P, Zhong ZW, Pecht M (2013) Copper wire bonding concerns and best practices. J Electron Mater. doi:10.1007/s11664-013-2576-1
4. Schneider-Ramelow M, Geißler U, Schmitz S et al (2013) Development and status of Cu ball/wedge bonding in 2012. J Electron Mater 42:558–595. doi:10.1007/s11664-012-2383-0
5. Appelt BK, Tseng A, Chen C-H, Lai Y-S (2011) Fine pitch copper wire bonding in high volume production. Microelectron Reliab 51: 13–20
6. Gan CL, Ng EK, Chan BL, Hashim U (2012) Technical barriers and development of cu wirebonding in nanoelectronics device packaging. J Nanomater 2012:1–7. doi:10.1155/2012/173025
7. Gan CL, Ng EK, Chan BL, T Kwuanjai, S Jakarin, Hashim U (2012) Wearout reliability study of cu and au wires used in flash memory fineline BGA package, 2012 I.E. 7th Int. Microsystems, Packag. Technol. Conf. pp 494–497
8. Gan CL, Toong TT, Lim CP, Ng CY (2010) Environmental friendly package development by using copper wirebonding. 34th IEEE CPMT IEMT, Malacca, 2010, pp. 1–5
9. Zhong ZW (2009) Wire bonding using copper wire. Microelectron Int 26:10–16
10. Breach CD (2010) What is the future of bonding wire? Will copper entirely replace gold? Gold Bull 43:150–168
11. Murali S, Srikanth N, Wong YM, Vath CJ (2006) J Mater Sci 42:615–623
12. Karpel A, Gur G, Atzmon Z, Kaplan WD (2007) Microstructural evolution of gold–aluminum wire-bonds. J Mater Sci 42:2347–2357
13. Drozdov M, Gur G, Atzmon Z, Kaplan WD (2008) Detailed investigation of ultrasonic Al–Cu wire-bonds: I Intermetallic formation in the as-bonded state. J Mater Sci 43:6029–6037
14. Drozdov M, Gur G, Atzmon Z, Kaplan WD (2008) Detailed investigation of ultrasonic Al–Cu wire-bonds: II. Microstructural evolution during annealing. J Mater Sci 43:6038–6048
15. Xu C, Breach CD, Sritharan T et al (2004) Oxidation of bulk Au–Al intermetallics. Thin Solid Films 462–463:357–362
16. Xu H, Liu C, Silberschmidt VV et al (2009) A re-examination of the mechanism of thermosonic copper ball bonding on aluminium metallization pads. Scr Mater 61:165–168
17. Xu H, Liu C, Silberschmidt VV et al (2011) Behavior of aluminum oxide, intermetallics and voids in Cu–Al wire bonds. Acta Mater 59: 5661–5673
18. Zeng Y, Bai K, Jin H (2013) Thermodynamic study on the corrosion mechanism of copper wire bonding. Microelectron Reliab. In Press
19. Gan CL, Ng EK, Chan BL, Hashim U (2012) Reliability challenges of Cu wire deployment in flash memory packaging. 2012 I.E. 7th Int. Microsystems, Packag. Technol. Conf. pp 498–501
20. Tan C, Daud A, Yarmo M (2002) Corrosion study at Cu–Al interface in microelectronics packaging. Appl Surf Sci 191:67–73

21. Uno T (2011) Microelectron reliab 51:148–156
22. Yamaji Y, Hori M, Ikenosako H, et al. (2011) IMC study on Cu wirebond failures under high humidity conditions. 2011 I.E. 13th Electron. Packag. Technol. Conf. IEEE, pp 480–485
23. Su P, Seki H, Ping C, et al. (2013) Effects of reliability testing methods on microstructure and strength at the Cu wire-Al pad interface. 2013 I.E. 63rd Electron. Components Technol. Conf., pp 179–185
24. Lu YH, Wang YW, Appelt BK, Lai YS, Kao CR (2011) Growth of CuAl intermetallic compounds in Cu and Cu (Pd) wire bonding. 2011 I.E. Electron. Components Technol. Conf., pp 1481–1488
25. Gan CL, Ng EK, Chan BL et al (2012) Wearout reliability and intermetallic compound diffusion kinetics of Au and PdCu wires used in nanoscale device packaging. J Nanomater 2012:1–9
26. Gan CL, Hashim U (2013) Reliability assessment and mechanical characterization of Cu and Au ball bonds in BGA package. J Mater Sci Mater Electron 24:2803–2811
27. Gan CL, Francis C, Chan BL, Hashim U (2013) Extended reliability of gold and copper ball bonds in microelectronic packaging. Gold Bull 46:103–115
28. Gan CL, Hashim U (2013) Superior performance and reliability of copper wire ball bonding in laminate substrate based ball grid array. Microelectron Int 30:169–175
29. Gan CL, Hashim U (2013) Comparative reliability studies and analysis of Au, Pd-coated Cu and Pd-doped Cu wire in microelectronics packaging. PLoS One 8:1–8
30. Gan CL, Francis C, Chan BL, Hashim U (2014) Future and technical considerations of gold wirebonding in semiconductor packaging—a technical review. Microelectron. Int. 31. In Press
31. Gan CL, Francis C, Chan BL, Hashim U (2013) Effects of wire type and mold compound on wearout reliability of semiconductor flash fineline BGA package. IEEE 8th Int. Microsystems, Packag. Assem. Circuits Technol. Conf. pp 297–301
32. Yu C-F, Chan C-M, Chan L-C, Hsieh K-C (2011) Cu wire bond microstructure analysis and failure mechanism. Microelectron Reliab 51:119–124
33. Mc Pherson JW (2013) Reliability physics and engineering: time-to-failure modeling, 2nd edn. Springer, New York
34. Gan CL, Hashim U (2013) Reliability assessment and activation energy study of Au and Pd-coated Cu wires post high temperature aging in nanoscale semiconductor packaging. J Electron Packag 135: 021010
35. JEDEC IPC STD 020 (2008) Moisture/reflow sensitivity classification for nonhermetic solid state surface mount devices